



Dual packed bed adsorption of sulphur dioxide from surface modified haematite / III-ferric oxide: characterization of the mass transfer zone



Albert Selvakumar Jeyapaul^{a,b}, Mahesh Ganesapillai^{c,*}

^a Research Scholar, School of Chemical Engineering, Vellore Institute of Technology, Vellore, 632014, Tamilnadu, INDIA

^b Lecturer, Chemical Engineering Department, College of Engineering and Technology, Samara University, Afar Region, ETHIOPIA

^c Professor, School of Chemical Engineering, Vellore Institute of Technology, Vellore, 632014, Tamilnadu, INDIA

ARTICLE INFO

Keywords:

Ferric oxide
Modified specific surface
Adsorption capacity
Atomic absorption spectroscopy

ABSTRACT

The adsorption process was adopted to separate SO₂ from surface modified haematite / III-ferric oxide with highly positive nano-particles. Ferric oxide was produced by precipitation at a different temperature rate. Adsorption of SO₂ was performed in a dual packed bed column with different process parameters such as temperature, adsorbate rate to achieve balance of isotherm. Characteristics of adsorption have been studied such as concentration gradient, exhaustion time T_{0.95}, mass transfer zone length (L_{MTZ}), breakthrough time T_{0.05} and constant rate. Chemisorption between the surfaces of ferric oxide activated and the targeted adsorbate SO₂ were strongly influenced between 45 and 50 °C. The adsorbent was analysed before and after the adsorption process using the X-Ray Diffraction Method (XRD), Atomic Adsorption Spectroscopy (AAS) to investigate adsorption properties such as porosity, specific surface area (152 m²g⁻¹), adsorption capacity and characterization. The study showed that the activated ferric oxide surface affects the adsorption process capacity more than other metal oxide surfaces. Higher specific surface area (558 m²g⁻¹) of ferric oxide activated adsorbed more SO₂ than non-activated ferric oxide at room temperature.

1. Introduction

Globally, six common air pollutants have been identified as major pollutants, which include SO₂, carbon monoxide, lead, nitrogen dioxide, carbon and dust (Eugene et al., 2007). According to the Environmental Protection Agency, scientists from universities around the globe have said that India has surpassed the United States in 2010 and has become the world's second-largest emitter of SO₂ after China. China has successfully lowered SO₂ emissions in its chemical industries through the use of various technologies (Fereshtee et al., 2018). The combustion of fossil fuels in chemical industries, power plants and individual homes emit such enormous quantities of dangerous SO₂ into the atmosphere, creating acid rain and causing human respiratory problems.

Short-term SO₂ exposure can lead to chest pain, shortness of breath and wheezing. Long-term exposure to SO₂ gas in combination with enormous quantities of particulate soot can lead to worsening of established cardiovascular disease, lung alterations and respiratory disease (Michael et al., 2019). Burning fossil fuels in chemical industries such as biomass, brown coal, gasoline, and natural gas is causing dust particulates, nitrogen oxides, and sulphur oxides to pollute the environment. It is doubtful that the use of such non-renewable energy

sources in industries and the everyday life of humans is now impossible (Prabhat KRai, 2016). The best solution to limit SO₂ emissions is therefore the acceptable application of technologies and the elimination of environmentally hazardous equipment substances resulting from the complete combustion of unwanted gasses (John et al., 2019). It is the worst precursor for a form of suspended particles that can affect the microphysical and optical properties of condensed nuages in the atmosphere. Emission of SO₂ particulates can be diluted and released into the atmosphere using stacks of tall flue gas and thereby producing acid rain. Immediate release of SO₂ into the atmosphere (Wei Lv et al., 2018) by the use of a large flue gas stack can be transformed into other compounds, which can damage the environment.

Treatment of SO₂ gas emissions has been attracted and increased focus has been given to chemical engineers as revised environmental issues impose high stringent regulations and therefore many approaches have been addressed to reduce SO₂ gas particulate emissions. Chemical manufacturing industries engaged in processes such as roasting, sulphide ores processing, smelting and power plants engaged in the combustion of large amounts of sulphur coal, fossil fuels and natural gas are the main sources of SO₂ gas emissions (Reinhold et al., 2013) and the greatest problem for chemical engineers is how to

* Corresponding author.

E-mail address: maheshgpillai@vit.ac.in (M. Ganesapillai).

<https://doi.org/10.1016/j.sajce.2020.06.008>

Received 20 February 2020; Received in revised form 12 June 2020; Accepted 25 June 2020

1026-9185/ © 2020 The Authors. Published by Elsevier B.V. on behalf of Institution of Chemical Engineers. This is an open access article under the CC BY-NC-ND license (<http://creativecommons.org/licenses/by-nc-nd/4.0/>).

effectively reduce SO₂ emissions in large industries. The biggest challenge for chemical engineers and industrialists is how to economically reduce SO₂ gas emissions in power plants and other chemical industries. There were several chemical processes approached to reduce emissions of SO₂ gases in industries based on research over a period of time. Such approached approaches for reducing SO₂ emissions were focused either on pollution preventiveness or on stopping long pipe handling of flue gases.

In small-scale industries, the handling of flue gas treatment is quite impractical and can lead to zero emissions of SO₂, instead of sulphur containing fuels, clean fuels should be used to achieve zero emissions of SO₂:

- Full sulphur separation from fuel: Hard coal should be thoroughly washed before it can be used in industrial combustion portion. Although there are many methods available for removing sulphur from fuel in the industries, the best method is desulphurizing and it should be done before firing in industries.
- Consume pure fuel: There are two methods of consuming pure fuel in industries; the first is to reduce the sulphur content to an reasonable value before it is combusted, and the second is to reduce the use of sulphur containing fuel in industries that are impossible now or in the near future, because industries mainly rely on sulphur-containing fossil fuels.
- Limit production and emit of SO₂ while combustion in industries: There have been many strategies, methods and procedures developed and introduced in industries to reduce SO₂ emissions, but very few of them are sold that are not environmentally friendly (Smith et al., 2005).

The surface area of an adsorbent can change the capacity of adsorption and can generally be defined as quantity if adsorbed on the adsorbent unit surface. α-Ferric oxide(α-Fe₂O₃) was selected as an adsorbent in this review, and the removal or separation of SO₂ is a polar and hydrophobic form of adsorbent (Bharat et al., 1996).

Analysis of engineering papers notes that chemical engineers, researchers, scientists and technologists have the authority to educate basics, methods, techniques and practical aspects of adsorption processes and help the environment to restrict the emission of SO₂ from combustion of fuels and flue gas in the chemical industries. The activated carbon fibre has tremendous potential to adsorb SO₂ due to its adsorption ability. In the chemical industry SO₂ gas has been used to adsorb fly ash as solid state adsorbent air defence technologies. Zeolites can be derived from fly ash, and use of solid waste from chemical industries was one of the effective techniques (Debora et al., 2017). Those zeolites of fly ash should be used to reduce SO₂ emissions. In this work, precipitation and thermal decomposition process provided SO₂ and ferric oxide to perform efficient adsorption processes with different parameters. After activation of ferric oxide, these adsorbents were used in dual bed columns to enrich base activities on the ferric oxide surface. In a dual packed bed, equilibrium isotherm was investigated to give more contact time between the adsorbent and the adsorbate. Following a tremendous adsorption process, adsorbent was analysed to know that adsorption capacity and balance was achieved on the ferric oxide surface (Shivaji Sircar, 1984).

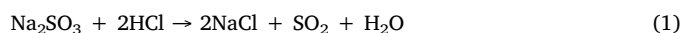
2. Materials and methods

2.1. Sulphur dioxide preparation

Small quantities of sodium sulphite were taken and weighed to measure the quantity of restricted reactant needed for the production of SO₂ gas. The calculated sodium sulphite quantity was moved into conical flask and its mouth was closed with a rubber cork. The rubber cork had two open and the first open was connected to a conical funnel while another was connected to a pipe line to allow the gas produced to pass to another conical flask already filled with a solution of hydrogen peroxides. The pipe line connecting the second conical flask should be

submerged in a solution diluted with hydrogen peroxide to produce 79 °C sulphuric acid (Schroeter, 2014). Second conical flask which has hydrogen peroxide temperature was maintained throughout the experiment by electrical heater which has inbuilt of magnetic stirrer. The second conical flask hydrogen peroxide solution was stirred till the completion of reaction between sodium sulphite and hydrochloric acid. Prepared diluted hydrochloric acid was transferred to the first conical flask containing sodium sulphite as a thin layer in order to prevent laboratory accidents and gradually full reaction.

The first conical flask was placed in a magnetic stirrer and the stirrer was turned on as soon as hydrochloric acid was introduced to initiate the reaction, and was allowed to rotate until the reaction was completed. When the reaction started by adding hydrochloric acid to sodium sulphite, SO₂ gas was released (Shanthi et al., 1994) and the gas produced was transferred to another conical flask containing a solution of hydrogen peroxide via a pipe line connecting two conical flasks. Created gasses, using rubber cork, were not allowed to escape from the conical flask. With the help of hydrogen peroxide at 79 °C, it was converted into sulphuric acid to analyse generated quantity of SO₂. After completion of the reaction pipe lines were dismantled and samples were taken from second conical flask to analyse the production of SO₂ using acid-base titration method. The below mentioned reactions (1) and (2) were used to produce and analyse SO₂.



2.2. Analysis of sulphur dioxide

The method of acid-base titration was used to analyse the quantity of sulphur dioxide released. Acid was the second conical flask sample, and the base was a solution of sodium hydroxide. Methyl red was used as a titration measure. Indicator from second conical flask was added into the sample, and the sample solution transformed into pale pink colour. Sodium hydroxide solution was titrated to coloured solution (Flavia et al., 2019). As soon as the required amount of sodium hydroxide was added to the sample, pink colour disappeared, which means the sample became neutral. After titration calculation part was performed to know the quantity of SO₂ generated as shown below (3)

$$\text{Normality of produced H}_2\text{SO}_4 = \frac{\text{NaOH volume} \times \text{Normality of NaOH}}{\text{Volume of sulphuric acid solution}} \quad (3)$$

In order to know the quantity of SO₂ present in the sample, the total quantity of SO₂ output, and the normality of extracted sulphuric acid was determined. The procedures were repeated with the same steps with full SO₂ reaction.

2.3. Ferric oxide preparation and activation

The process of thermal decomposition was employed to manufacture ferric oxide from ferrous sulphate heptahydrate. Sodium carbonate was the limited reactant which can react with ferrous sulphate heptahydrate to produce ferric oxide. Initially ferrous sulphate heptahydrate solution was prepared by adding distilled water to the known quantity of ferrous sulphate heptahydrate in a conical flask with constant stirring. The sodium carbonate salt was taken and diluted into a second conical flask. This diluted solution is preheated to 71 °C (Dong Fu et al., 2008) and kept temperature until reaction between reactants is completed. Pre heated diluted solution stock was put into the first conical flask that had the ferrous sulphate solution and started reaction.

The first conical flask was put in a magnetic stirrer and turned on as soon as the sodium carbonate in the first flask was added. Using a pH metre, pH was measured in order to know the completion of the

reaction. Sodium carbonate was sent as thin layer into the first conical flask and constantly stirred until pH reached 9.5. Precipitation was formed and this semi-solid material was filtered from the required solid content to separate the sodium sulphate solution (Meng et al., 1995). Solid content was washed thoroughly with distilled water, and the solid content was transferred to silica crucible. In order to obtain ferric oxide it was put in muffle furnace to do calcinations operation. Three different heating rates were introduced to ensure the quality of the ferric oxide by repeating the same procedure. When muffle furnace reached 500 °C, the calcination process was stopped.

The calcined material was thoroughly washed with distilled hot water to remove undesirable excess material and kept it in the muffle furnace to reach 110 °C, and the temperature was maintained for six hours to modify the haematite surface. Produced ferric oxide with mixture of sodium hydroxide and ethanol solution was allowed to enrich the pH at 80 °C. On the other hand, sodium sulphate solution was transferred to another conical flask, and evaporation process started to obtain sodium sulphate salt crystals. The production of ferric oxide by thermal decomposition process is one of the main advantages (National Center for Biotechnology Information, 2020). Below is the flow sheet for processing the ferric oxide. Fig. 1 shows the pictorial representation for the ferric oxide preparation cycle.

2.4. Ferric oxide analysis

Prepared ferric oxide by thermal decomposition process was sent to X-Ray Diffraction (XRD) method for analysing the purity of ferric oxide and Atomic Absorption Spectroscopy (AAS) for knowing the percentage of iron content in ferric oxide. The ferric oxide was activated with a mixture of sodium hydroxide and ethanol solution after study by XRD (Azza et al., 2019) and AAS to enrich pH at 80 °C. After activated with chemicals pH was measured to know the activation capacity to capture SO₂.

2.5. Adsorption of sulphur dioxide in dual packed bed

Arrangement to perform SO₂ adsorption in dual packed bed column is very simple and is shown in Fig. 2 below. Prepared diluted hydrochloric acid was connected to the suction of a constant flow pump, and the pump delivery was linked to a two open conical flask that has sodium sulphite within. A tube was attached between the bottom of the adsorption column and the conical flask mouth. The top of the adsorption column was attached to a wire, resulting in a dip in the solution of hydrogen peroxide to trap excess SO₂ from the column of adsorption.

Adsorption column had double packed bed filled with activated ferric oxide produced. Adsorptions were performed in dual packed bed on the surface of ferric oxide, and excess SO₂ after adsorption went to the absorption section where hydrogen peroxide was placed. The main purpose of using dual-packed bed column is to reduce the escape of SO₂ from adsorption and the arrangement provides greater contact time between adsorbent and adsorbent. Excess quantity of SO₂ was converted into sulphuric acid and the quantity was analysed using titration method and measured to know the ability of activated ferric oxide to adsorb (Jun et al., 2009).

2.6. Mass transfer zone

Adsorption mass transfer zone is gradient high in adsorbate concentration between inlet and outlet, and at the end there will be almost no mass transfer zone, which means that the adsorbent has reached equilibrium. Therefore there was no more porous media available to adsorb SO₂ on the activated ferric oxide surface (Jian et al., 2019). Here in this research exhaustion time (T_{0.95}) and breakthrough time (T_{0.05}) was measured and calculated to know mass transfer zone. Mass transfer zone length (L_{MTZ}) was calculated from Eq. (4).

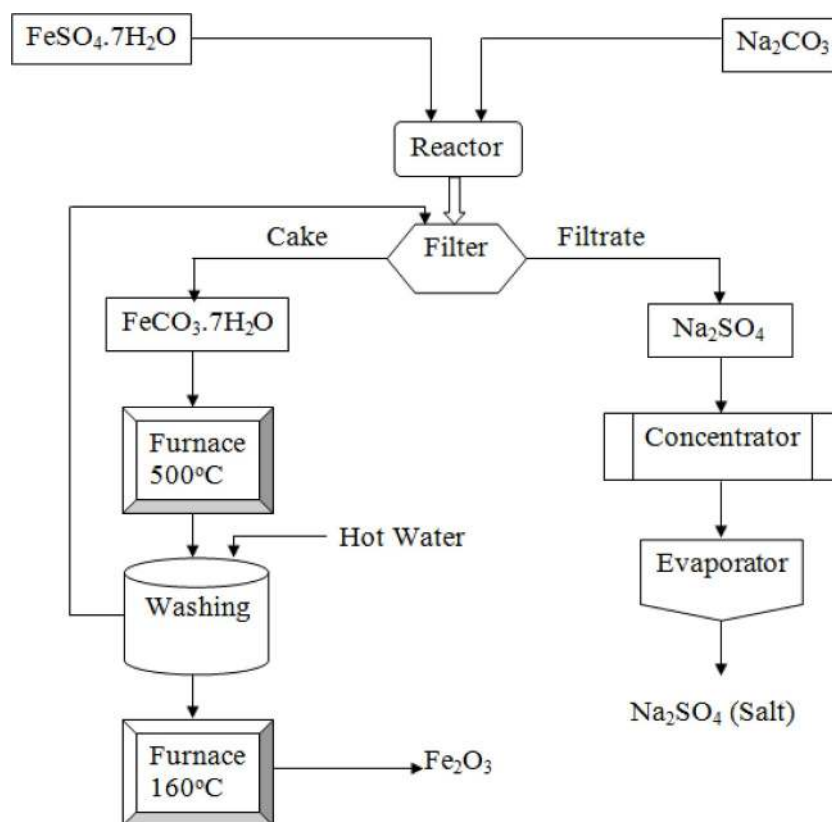


Fig. 1. Process flow diagram of ferric oxide preparation.

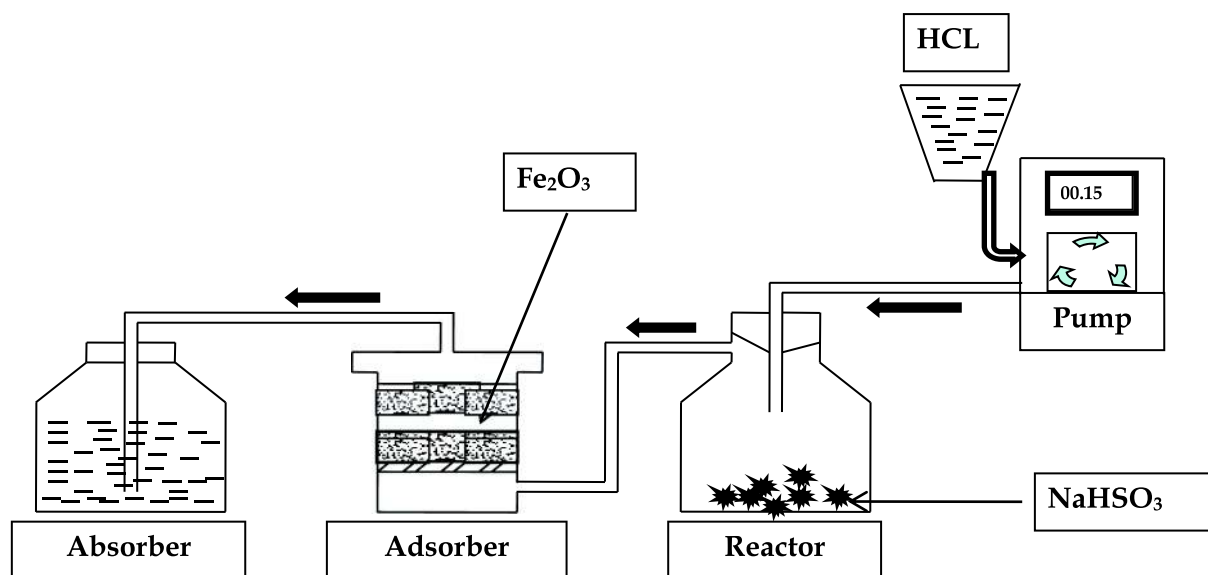


Fig. 2. Schematic flow diagram of adsorption process.

$$L_{MTZ} = \frac{(T_{0.95} - T_{0.05}) \times L}{(T_{0.95} + T_{0.05})/2} \quad (4)$$

The measuring unit for mass transfer zone length in cm, and min are used for breakthrough and exhaust time. Breakthrough time for single-phase gas adsorption in dual-packed bed column is given below in Eq. (5).

$$T_{0.95} = \frac{\rho_b \times W \times L}{C_0 \times U} - \frac{\rho_b \times W \times \ln\left(\frac{C_0 - C_{0.05}}{C_{0.95}}\right)}{C_0 \times K} \quad (5)$$

Ferric oxide bulk density (ρ_b) was measured several times in gcm^{-3} and average was taken into account to calculate breakthrough time. Adsorption capacity (W) was calculated by knowing the quantity of SO_2 gas adsorbed on surface of ferric oxide in relation to known quantity of ferric oxide placed in the dual packed bed. After the breakthrough time calculation a graph was diagrammed between the length of the mass transfer zone (Moamen S Refat, 2014) and the breakthrough time to know the adsorption rate constant (K) specification from the graph slope.

2.7. Specific surface area of ferric oxide and activated ferric oxide

A known quantity of ferric oxide was taken in clay bowl and calcinated for two hours at 300°C in the presence of atmospheric air (Ru-Ling Tseng, 2007) and mixed with 5 percent of sodium hydroxide and ethanol solution by weight. The mixture is placed in the same clay bowl and left natural for a night to evaporate excess solvents. The prepared material is called activated ferric oxide and XRD analysed the sample to determine the specific area of the surface. The Sauter's (M Streat et al., 2008) Eq. (6) is used to calculate the particular ferric oxide surface area.

$$\text{Specific surface area} = \frac{6000}{\rho \times D} \quad (6)$$

3. Results and discussion

3.1. Ferric oxide density

A known quantity of water was poured into a measuring cylinder and weighed quantity of activated ferric oxide prepared placed in the same flask. Once ferric oxide was added to the water content, small

volume changes were observed and the density of ferric oxide was measured (Farah et al., 2011) using the following Eq. (7).

$$\text{Density} = \frac{\text{weighed quantity of ferric oxide}}{\text{change of volume}} \quad (7)$$

The calculated density of activated Fe_2O_3 is 5.10 g cm^{-3} and this value is almost equivalent to theoretical density of the same. The average activated ferric oxide density was calculated by repeating same procedure with different heating rates in the calcinations section in thermal decomposition process and the value was 5.13 g cm^{-3} .

3.2. Consequences of reaction analysis

The theoretical and experimental analysis of materials used in the production of ferric oxide was based on the following chemical reactions (8,9,10 and 11) and method



The main excess reactant for producing ferric oxide by thermal decomposition method is sodium carbonate, and the quantity required was calculated based on the above mentioned reactions and produced ferric oxide. In addition, pH analysis was performed to determine the completion of the chemical reaction. Acid-base was the type of reaction between the ferrous sulfate heptahydrate and sodium carbonate. Therefore, pH was controlled for each and every small quantity of diluted sodium carbonate applied to the ferrous sulphate heptahydrate solution to be able to complete the reaction (Juana et al., 2016). Here ferrous sulphate heptahydrate served as acid and the base was sodium carbonate. When the theoretical amount of sodium carbonate needed was added into ferrous sulphate, the solution mixture did not reach an equivalent level, so there was a delay.

A particular reason for the lag in reaction between strong acid and weak base was conjugate base production since the base used was weak in ferric oxide production (Kakavandi et al., 2013). The lag was balanced with a little more over reactant added. A graph (Fig. 3) was plotted between observed pH changes in the mixture, while the reaction and quantity of the sodium carbonate solution added to the limited reactant was identified and the completion of the reaction at the

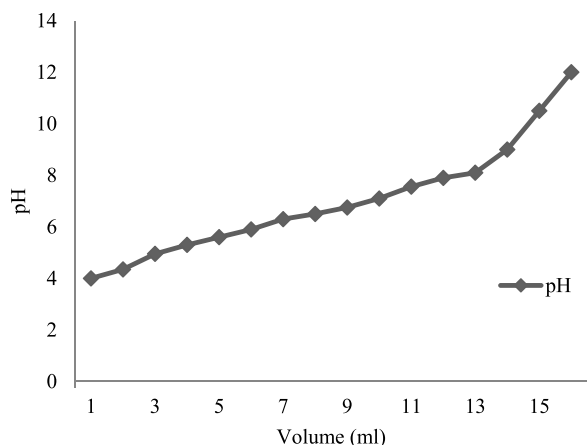


Fig. 3. Reaction analysis between ferrous sulphate heptahydrate and sodium carbonate.

equivalent point was identified.

3.3. Analysis by atomic absorption spectroscopy

Atomic absorption spectroscopy has been used to analyse elements present in the prepared ferric oxide and to learn the iron content in it based on the law of Beer-Lambert. In order to know the iron concentration in the normal and unknown ferric oxide solution was made in the same way and kept in spectroscopy. Based on the observance of the AAS study (Lancok et al., 2009), Fig. 4 is plotted and it represents the graph between iron particle concentration and absorption from the unknown solution and projected iron concentration in ferric oxide.

The concentration of iron presented in the prepared ferric oxide was observed from an AAS analysis. Based on the linearized equation from the plotted graph, iron quantity present in the ferric oxide was 66.8%.

3.4. X-Ray diffraction analysis

Crystallinity of ferric oxide thin film has been calculated from X-Ray Diffraction (XRD) analysis. The prepared ferric oxide structure was hexagonal, and polycrystalline was the nature of the ferric oxide. The natural structure was very clear when temperatures increased while ferric oxide was being prepared in a muffle furnace.

Intensity and peak angle were observed from XRD analysis (S Veena et al., 2015), and a graph was plotted between them, shown in

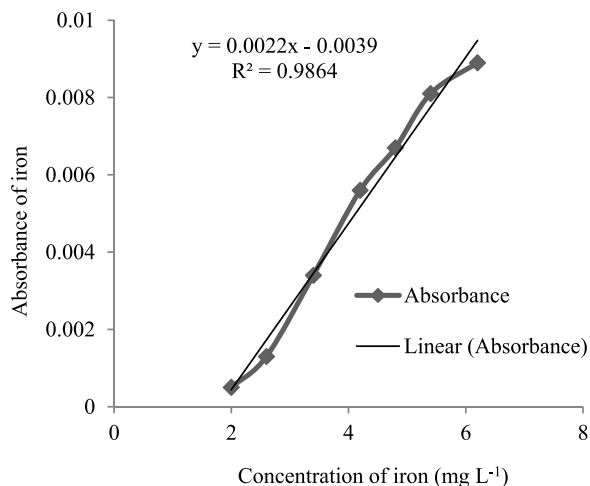


Fig. 4. Analysis of iron content in ferric oxide by Atomic Absorption Spectroscopy (AAS).

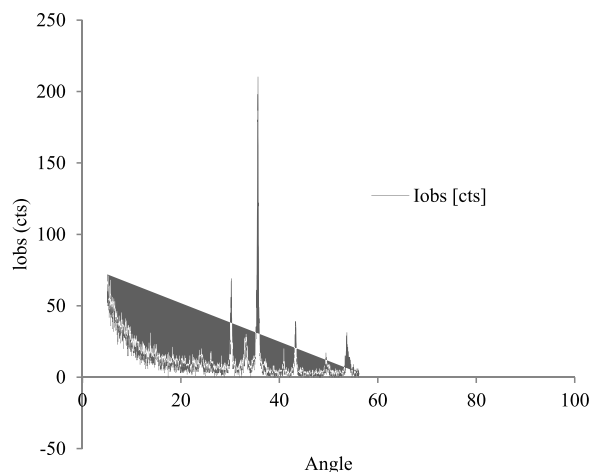


Fig. 5. XRD analysis of ferric oxide under the arc current of 32 A and temperature 25 °C.

Fig. 5 to understand ferric oxide properties such as purity and particle size. A lot of sharp peaks appeared in the graph and it means there was no defect in the ferric oxide crystals. The average crystal size of the ferric oxide was determined by the equation described below (12)

$$D = \frac{0.9\lambda}{\beta \cos\theta} \quad (12)$$

The range of size of the ferric oxide crystal was between 20 and 22 nm. XRD found the specific area of ferric oxide and activated ferric oxide and used the equation to calculate the specific area of the surface (13).

$$\text{Specific surface area} = \frac{6000}{\rho \times D} \quad (13)$$

The specific surface area of ferric oxide and activated ferric oxide was found to be 152 and 526 m²g⁻¹ respectively.

3.5. Analysis of reaction time to produce sulphur dioxide

The known quantity of sodium sulphite is reacted with hydrochloric acid to obtain SO₂ gas. The produced quantity of SO₂ was analysed and calculated for every 5 min of the reaction. The first three experiments were conducted in five min intervals and the last three experiments were carried out in 15 min intervals. Acid-base titration method was used to analyse produced SO₂ content and observations were plotted in graph.

In experiments and graph the reaction time was estimated from the observation. Fig. 6 shows that the reaction time is between 10 and 15 min, so experiments should be repeated between 10 and 15 min at 1 min intervals to find exact reaction time. The experiment provided maximum amount of SO₂ at 523 ppm.

The completion of the sodium sulphite and hydrochloric reaction was approximately 14 min since the graph shows the constant line after 14 min and the maximum amount of SO₂ released by the experiment was 522 ppm. The full exact reaction time is estimated in Fig. 7. Nevertheless, the same experiment should be repeated to know every single SO₂ output. Similar amount of SO₂ was sent to the adsorption column to adsorb the ferric oxide surface.

3.6. Sulphur dioxide adsorption on surface of ferric oxide

Three separate adsorption column SO₂ inlet concentrations were set as 152.5, 130.4 and 112.8 ppm and adsorption on the activated ferric oxide surface was carried in the adsorption column of dual packed beds. The height of the first double bed was 5 cm and the distance between

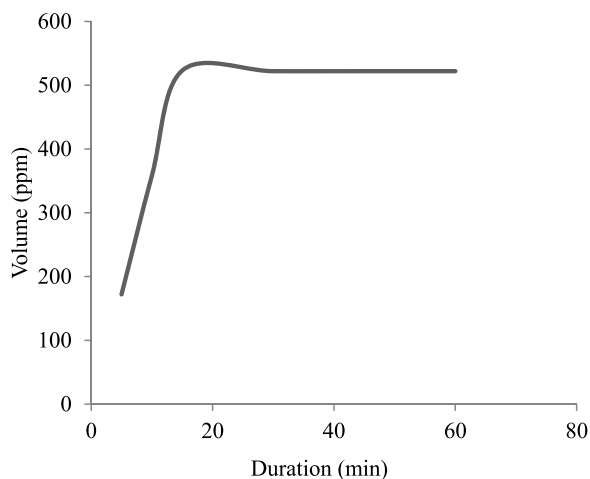


Fig. 6. Completion of reaction analysis of SO_2 .

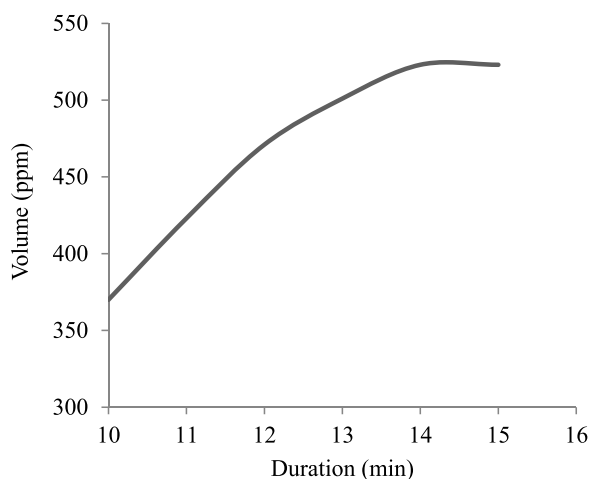


Fig. 7. Exact completion of reaction analysis of SO_2 .

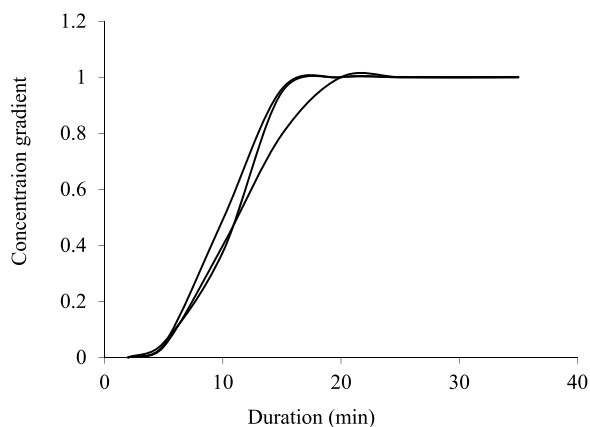


Fig. 8. Adsorption of SO_2 on 5 cm height of dual packed bed of ferric oxide.

the two beds was 5 cm. Observation on adsorption has been used to plot a graph between duration of the reaction and concentration gradient as depicted in Fig. 8.

Observation of SO_2 adsorption was used to plot a graph between the length of the reaction and the concentration gradient at the height of the dual bed and the distance between the dual beds was 5 cm. The high ferric oxide surface area allowed large amounts of adsorption when the concentration of SO_2 at the inlet was also high. As there was no change in temperature and pressure (Hoghong et al., 2019) during the process,

the concentration gradient was gradually raised to 5 min. SO_2 adsorption on activated ferric oxide was high between 5 and 20 min and the break-through started in 6 min and reached a balance of 15–17 min (Fig. 8). Adsorbent sample was sent to the section of analysis after the adsorption phase to know the adsorption power. The procedure was repeated with all three concentrations of the same SO_2 inlet and sent to another adsorption column, which had a dual packed bed of 10 cm in length. The distance between the columns of the packed beds was also 5 cm in length.

The height of packed bed is changed from 5 to 10 cm and notified adsorption of adsorption. Based on observation a graph was drafted between the length of the reaction and the concentration gradient. The same gap 5 cm is maintained between the packed bed columns. Although the process procedure was identical, different concentration gradients were identified and equilibrium was achieved between 23 and 25 min, meaning mass transfer zone length (L_{MTZ}) was delayed to nearly zero (David et al., 2015). Since the size and capacity of the adsorption column was adsorbed on the activated ferric oxide surface little more than the previous huge amount of SO_2 . Procedures were repeated with 15 cm long dual packed bed and noticed changes on equilibrium curves (Fig. 9).

SO_2 adsorption observation was used to plot a graph (Fig. 10) of 15 cm between the duration of the reaction and the concentration gradient with the height of the dual bed and 5 cm between the dual beds. In the third dual bed, SO_2 diffused more and almost all quantities were adsorbed by activated ferric oxide since the height of the packed bed is more compared to the previous two. This is the main advantage and significance of the column of dual packed bed adsorption and it gave more contact time to the adsorbent and adsorbate. Instead of offering more retention time to efficiently adsorb SO_2 this structure is useful for efficient handling of SO_2 adsorption. As soon as concentration expanded adsorption capacity also expanded which added benefit to the process. Breakthrough was started late and equilibrium often delayed as a result. In Fig. 10, high adsorption capacity was noticed in the overall adsorption process as soon as the achievement of equilibrium delayed a little in the column.

The higher dual packed bed column showed little pressure drop and it could be one of the reasons for delay in achieving equilibrium. Based on the observation duration of the mass transfer zone (Fig. 11), the mass transfer zone was found to decrease as soon as the breakthrough period was delayed.

3.7. Temperature effects on SO_2 adsorption

Initially, SO_2 concentration of 200 ppm was fed into the adsorption column where ferric oxide was kept in a packed bed and room temperature throughout the adsorption process was maintained. Full fusion

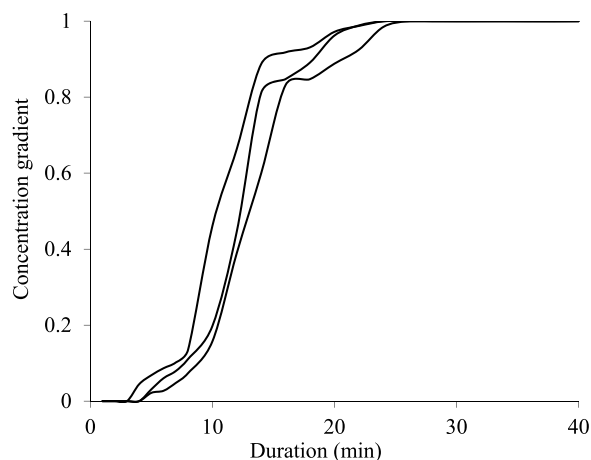


Fig. 9. Adsorption of SO_2 on 10 cm height of Ferric oxide dual bed.

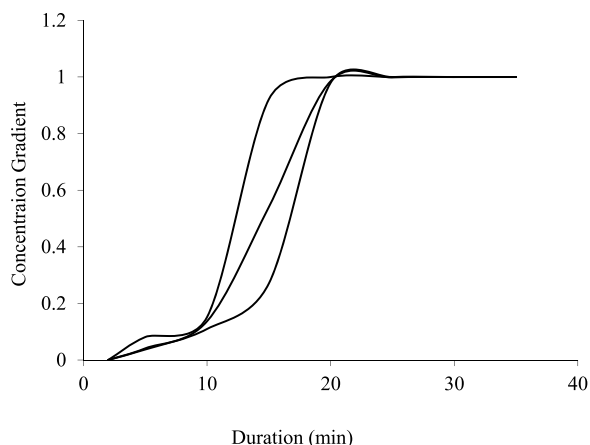


Fig. 10. Adsorption of SO₂ on 15 cm height of Ferric oxide dual bed.

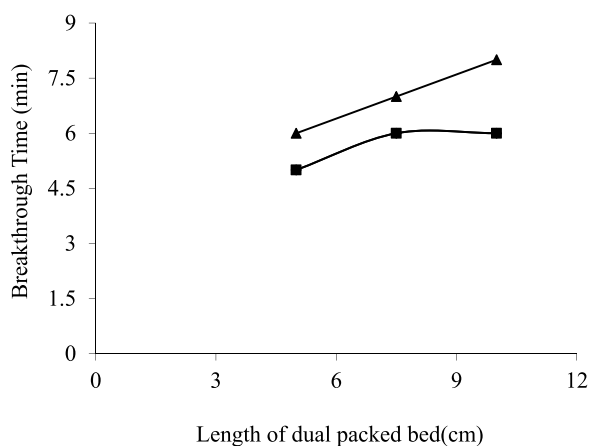


Fig. 11. Breakthrough time with respect to dual packed column length.

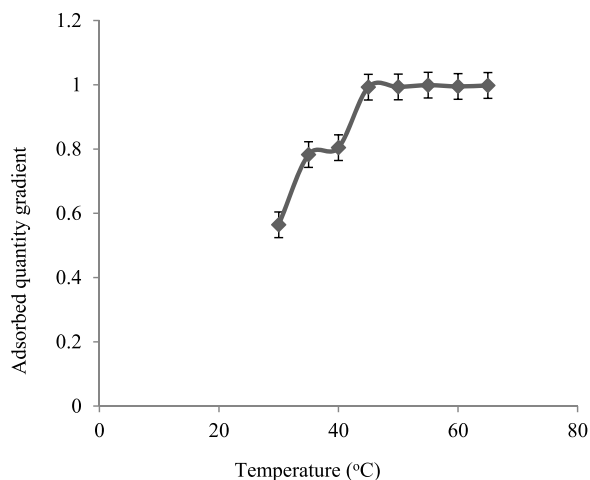


Fig. 12. Effect of temperature on SO₂ adsorption by activated ferric oxide.

of SO₂ and ferric oxide was observed when relatively higher temperatures and rapid equilibrium were reached.

Specific temperature levels were inserted into the adsorption column and found that comparatively higher temperatures than room temperatures (Fig. 12) play a major role in achieving rapid equilibrium, however, the temperature between 45 and 50 °C is sufficient to achieve an equilibrium which is the best parameter to adsorb SO₂ and the complete adsorption process may not require additional heat energy to achieve adsorption equilibrium. Compared to other metal oxides such

as zeolite, Al₂O₃ (Diana et al., 2008) and activated carbon, activated ferric oxide can achieve equilibrium at relatively low temperatures, which is an added advantage for process industries, making it possible to adsorb lower concentrations of SO₂ at relatively low temperatures.

4. Conclusions

Adsorbent, ferric oxide was prepared by thermal decomposition process, which helped to remove excess acidity and then activated with help of sodium hydroxide and ethanol solution. Physical properties of prepared ferric oxide were investigated with the help of X-Ray Diffraction analysis and concentration of presents in the produced ferric oxide was found by atomic absorption spectroscopy. Each gram of modified prepared ferric oxide helped quickly to adsorb 220 ppm of SO₂, thus breakthrough delayed. However, modified ferric oxide enriched the capacity of adsorption, equilibrium attained very fast in the range of 10–20 min though length of dual packed bed is more. Dual packed bed has given more contact time between SO₂ and ferric oxide and it was one of the reasons why exhaustion time delayed quietly. Length of mass transfer zone (L_{MTZ}) was decreased as soon as SO₂ concentration increased from 220 ppm to 520 ppm. XRD shown that the crystallography of produced activated ferric oxide was clear and there was less bias in particle size. The average size of produced ferric oxide was 20–25 nm and it shows that the produced ferric oxide is belongs to α -Fe₂O₃(haematite) which is strong in stability and hydrophobic. Inlet concentration and rate of SO₂ played a main role in throughout adsorption process. Effects of inlet concentration, temperature effects and length of dual packed bed column on SO₂ adsorption were studied, and noticed that the best parameter to perform SO₂ adsorption is relatively moderate temperature between 45 and 50 °C and initial inlet concentration should be lower than 200 ppm. This adsorption method and production of ferric oxide could be useful to chemical industries to limit SO₂ emission completely when the concentration of SO₂ is low.

Declaration of Competing Interest

None.

References

- Mazrouaa, Azza M, Mohamed, Manal G, Fekry, Mohamed, 2019. Physical and magnetic properties of iron oxide nanoparticles with a different molar ratio of ferrous and ferric. Egypt. J. Pet. 28 (2), 165–171. <https://doi.org/10.1016/j.ejpe.2019.02.002>.
- Bharat, G.K., Yenkie, M.K.N., Natarajan, G.S., 1996. Influence of physico-chemical characteristics of adsorbent and adsorbate on competitive adsorption equilibrium and kinetics. In: LeVan, M.D. (Ed.), Fundamentals of Adsorption. The Kluwer International Series in Engineering and Computer Science 356 Springer, Boston, MA. https://doi.org/10.1007/978-1-4613-1375-5_10.
- Bahrin, David, Subagio, Susanto, Herri, 2015. Effect of regeneration temperature on particle characteristics and extent of regeneration of saturated SO₂-adsorption of CuO/ γ -Al₂O₃ adsorbent. Procedia Chem. 16, 723–727. <https://doi.org/10.1016/j.proche.2015.12.020>.
- Strossi Pedrolo, Débora Regina, de Menezes Quines, Luci Kelin, Souza, Guilhermede, Romeu Marcilio, Nilson, 2017. Synthesis of zeolites from Brazilian coal ash and its application in SO₂ adsorption. J. Environ. Chem. Eng. 5 (5), 4788–4794. <https://doi.org/10.1016/j.jece.2017.09.015>.
- Fu, Dong, Wren, J Clara, 2008. Preparation and characterization of ferric oxyhydroxide and ferric oxide thin films by direct-hydrolysis deposition. J. Nucl. Mater. 374 (1–2), 116–122. <https://doi.org/10.1016/j.jnucmat.2007.07.014>.
- Cairncross, Eugene K, John, Juanette, Zunckel, Mark, 2007. A novel air pollution index based on the relative risk of daily mortality associated with short-term exposure to common air pollutants. Atmos. Environ. 41 (38), 8442–8454. <https://doi.org/10.1016/j.atmosenv.2007.07.003>.
- Kanwal, Farah, Siddiqi, Saadat Anwar, Batool, Aisha, Imran, M., Mushtaq, Waheed, Jamil, Tahir, 2011. Synthesis of polypyrrole–ferric oxide (PPy–Fe₂O₃) composites and study of their structural and conducting properties. Synth. Met. 161 (3–4), 335–339. <https://doi.org/10.1016/j.synthmet.2010.12.001>.
- Emami, Fereshteh, Masiol, Mauro, Hopke, Philip K, 2018. Air pollution at Rochester, NY: long-term trends and multivariate analysis of upwind SO₂ source impacts. Sci. Total Environ. 612, 1506–1515. <https://doi.org/10.1016/j.scitotenv.2017.09.026>.
- Braghirolli, Flavia Lega, Bouafif, Hassine, Koubaa, Ahmed, 2019. Enhanced SO₂ adsorption and desorption on chemically and physically activated biochar made from wood residues. Ind. Crops Prod. 138, 111456. <https://doi.org/10.1016/j.indcrop.2019.06>.

- 019.
- Yi, Honghong, Ma, Chuanbo, Tang, Xiaolong, Zhao, Shunzheng, Yang, Kun, Sani, Zaharaddeen, Song, Lingling, Zhang, Xiaodong, Han, Wen, 2019. Synthesis of MgO at CeO₂-MnO_x core shell structural adsorbent and its application in reducing the competitive adsorption of SO₂ and NO_x in coal-fired flue gas. *Chem. Eng. J.* 372, 129–140. <https://doi.org/10.1016/j.cej.2019.04.120>.
- Ren, Jian, Xue, Yanyan, Wang, Lin, 2019. SO₂ gas adsorption on the transition metal (Pd, Ag, Au and Pt) -doped monolayer MoSe₂: a first-principles study. *Chem. Phys. Lett.* 733, 136631. <https://doi.org/10.1016/j.cplett.2019.136631>.
- Balmes MD, John R, 2019. Household air pollution from domestic combustion of solid fuels and health. *J. Allergy Clin. Immunol.* 143 (6), 1979–1987. <https://doi.org/10.1016/j.jaci.2019.04.016>.
- ZHAO, Jun, YAO, Shanqing, LIN, Dongqiang, 2009. Adsorbents for expanded bed adsorption: preparation and functionalization. *Chin. J. Chem. Eng.* 17 (4), 678–687. [https://doi.org/10.1016/S1004-9541\(08\)60263-3](https://doi.org/10.1016/S1004-9541(08)60263-3).
- Kakavandi, B., Jonidi, A., Rezaei, R., 2013. Synthesis and properties of Fe₃O₄-activated carbon magnetic nanoparticles for removal of aniline from aqueous solution: equilibrium, kinetic and thermodynamic studies. *J. Environ. Health Sci. Eng.* 10, 19. <https://doi.org/10.1186/1735-2746-10-19>.
- Lancok, A., Klementova, M., Bezdicka, P., Migliorini, M., 2009. Characterization of magnetic iron oxide nanoparticles. In: Kuzmann, E., Lázár, K. (Eds.), *ISIAME 2008*. Springer, Berlin, Heidelberg. https://doi.org/10.1007/978-3-642-01370-6_11.
- Streat, M., Hellgardt, K., Newton, N.L.R., 2008. Hydrous ferric oxide as an adsorbent in water treatment: part 1. Preparation and physical characterization. *Process Saf. Environ. Prot.* 86 (1), 1–9. <https://doi.org/10.1016/j.psep.2007.10.007>.
- Ouyang, Meng, Hiraoka, Hiroyuki, 1995. Preparation and characterization of iron oxide films by the excimer laser ablation of poly(ferric methacrylate). *Mater. Sci. Eng.: B* 34 (2–3) 188–19. [https://doi.org/10.1016/0921-5107\(95\)01246-X](https://doi.org/10.1016/0921-5107(95)01246-X).
- Brauer, Michael, Sarath, K., Guttikunda, Nishad, K.A., Dey, Sagnik, Sachchida, N., Tripathi, Martin, Randall V, 2019. Examination of monitoring approaches for ambient air pollution: a case study for India. *Atmos. Environ.* 216, 116940. <https://doi.org/10.1016/j.atmosenv.2019.116940>.
- Refat, Moamen S, 2014. Preparation of manganese(II), chromium(III) and ferric(III) oxides nanoparticles in situ metal citraconate complexes frameworks. *Spectrochim. Acta Part A: Mol. Biomol. Spectrosc.* 133 281–29. <https://doi.org/10.1016/j.saa.2014.05.066>.
- National Centre for Biotechnology Information. Pubchem database. ferric oxide, CID = 56841934, <https://pubchem.ncbi.nlm.nih.gov/compound/Ferric-oxide> (accessed on June 7, 2020).
- Rai, Prabhat K, 2016. Chapter two - adverse health impacts of particulate matter, bio-magnetic monitoring of particulate matter. In: *In the Indo-Burma Hotspot Region*, pp. 15–39. <https://doi.org/10.1016/B978-0-12-805135-1.00002-0>.
- Spörl, Reinhold, Maier, Jörg, Scheffknecht, Günter, 2013. Sulphur oxide emissions from dust-fired oxy-fuel combustion of coal. *Energy Procedia* 37, 1435–1447. <https://doi.org/10.1016/j.egypro.2013.06.019>.
- Tseng, Ru-Ling, 2007. Physical and chemical properties and adsorption type of activated carbon prepared from plum kernels by NaOH activation. *J. Hazard. Mater.* 147 (3), 1020–1027. <https://doi.org/10.1016/j.jhazmat.2007.01.140>.
- Veena, S., Gopal, R., Mini, V., Bena Jothy, I., Joe, Hubert, 2015. In: *Synthesis and Characterization of Iron Oxide Nanoparticles using DMSO as a Stabilizer*. Materialstoday: Proceedings. 2. pp. 1051–1055. <https://doi.org/10.1016/j.matpr.2015.06.036>.
- Schroeter, L.C., 2014. *Sulphur Dioxide: Applications in Foods, Beverages, and Pharmaceuticals*. Elsevier Science, Saint Louis.
- Shanthi, K., Balasubramanian, N., 1994. Method for the sampling and analysis of sulphur dioxide. *Presenius. J. Anal. Chem.* 351, 685–686. <https://doi.org/10.1007/BF00323348>.
- Sircar, Shivaji, 1984. New adsorption isotherm for energetically heterogeneous adsorbents. *J. Colloid. Interface Sci.* 98 (2), 306–318. [https://doi.org/10.1016/0021-9797\(84\)90156-5](https://doi.org/10.1016/0021-9797(84)90156-5).
- Smith, S.J., Pitcher, H., Wigley, T.M.L., 2005. Future sulphur dioxide emissions. *Clim. Chang.* 73, 267–318. <https://doi.org/10.1007/s10584-005-6887-y>.
- Lv, Wei, Fan, Xiaohui, Gan, Min, Ji, Zhiyun, Chen, Xuling, Yao, Jiawen, Jiang, Tao, 2018. Investigation on activated carbon removing ultrafine particles and its harmful components in complex industrial waste gas. *J. Clean Prod.* 201, 382–390. <https://doi.org/10.1016/j.jclepro.2018.08.064>.